Patterned Transparent Conductive Au Films through Direct Reduction of Gold Thiocyanate

*Ahiud Morag, Natalya Froumin, Dimitry Mogiliansky, Vladimir Ezersky, Edith Beilis, Shachar Richter, and Raz Jelinek**

Construction of structurally defined, patterned metal films is a fundamental objective in the emerging and active field of bottom-up nanotechnology. A new strategy for constructing macroscopically organized Au nanostructured films is presented. The approach is based upon a novel phenomenon in which incubation of water-soluble $Au(SCN)_4^{1-}$ complex with amine-displaying surfaces gives rise to spontaneous crystallization and concurrent reduction, resulting in the formation of patterned metallic gold films. The Au films exhibit unique nanoribbon morphology, likely corresponding to aurophilic interactions between the complex moieties anchored to the amine groups through electrostatic attraction. Critically, no external reducing agents are needed to initiate or promote formation of the metallic Au films. In essence, the thiocyanate ligands provide the means for surface targeting of the complex, guide the Au crystallization process and, importantly, donate the reducing electrons. It is shown that the Au films exhibit electrical conductivity and high transparency over a wide spectral range, lending the new approach to possible applications in optoelectronics, catalysis, and sensing. In a broader context, a new gold chemistry route is presented in which ligand-enabled crystallization/reduction could open the way to a wealth of innovative reaction pathways and applications.

1. Introduction

Fabrication of thin, transparent conductive electrodes (TCEs) which would furthermore be inexpensive, robust, and exhibit scalable surface areas is a highly sought albeit challenging goal in optoelectronic, photovoltaic, and nanophotonics research and development.[1,2] In particular, fabrication schemes that might replace the commonly used indium tin oxide (ITO) technology are intensely sought due to the high cost and practical limitations of ITO-based TCEs.[1] While most currently fabricated micro- and nanoelectronic devices are produced via "top-down" lithography methods,[3] "bottom-up" approaches have emerged as promising alternatives for generation of organized nanostructures and electronic components.[4] Bottom-up techniques generally rely upon molecular self-assembly phenomena to produce defined structures that could be practically utilized.[5,6]

Varied studies have focused on self-assembly of gold nanostructures as a versatile and powerful means for creating patterned conductive surfaces. The propensity of Au ions to self-assemble and undergo reduction into colloids and NPs, however, poses distinct barriers for utilizing conventional gold chemistry for creating structurally defined, organized thin films. Patterned gold films can be assembled with the use of NPs organized on surfaces through chemical derivation of the particle surface[7] and/or the substrate supporting the film growth,[8–10] or through the aid of physical templates.[5,11–14] These approaches exhibit shortcomings, both conceptually as well as technically. Specifically, Au NP synthesis and surface derivatization are often multi-step procedures and introduce certain variability in term of product uniformity. In addition, in many cases chemical treatment of NP-based films is further required after surface deposition of the NPs, presenting additional experimental parameters to modify and optimize. Furthermore, on a fundamental basis, the rapid reduction of ionic gold into metal NPs severely restricts the possibility to control the structural features and spatial, long-range organization of the metal assemblies.

We present a new strategy for constructing TCEs through spontaneous, single-step formation of macroscopically organized Au nanostructured films. The approach is based upon incubation of water-soluble $Au(SCN)_4^{1-}$ complex with amine-displaying surfaces, resulting in crystallization and

A. Morag, Prof. R. Jelinek
Department of Chemistry
Ben Gurion University of the Negev
Beer Sheva 84105, Israel
E-mail: razj@bgu.ac.il
A. Morag, Dr. N. Froumin, Dr. D. Moglilansky, Dr. V. Ezersky, Prof. R. Jelinek
Ilsa Katz institute for Nanotechnology
Ben Gurion University of the Negev
Beer Sheva 84105, Israel
E. Beilis, Dr. S. Richter
Center for Nanoscience and Nanotechnology
Tel Aviv University
Tel Aviv 69978, Israel

DOI: 10.1002/adfm.201300881

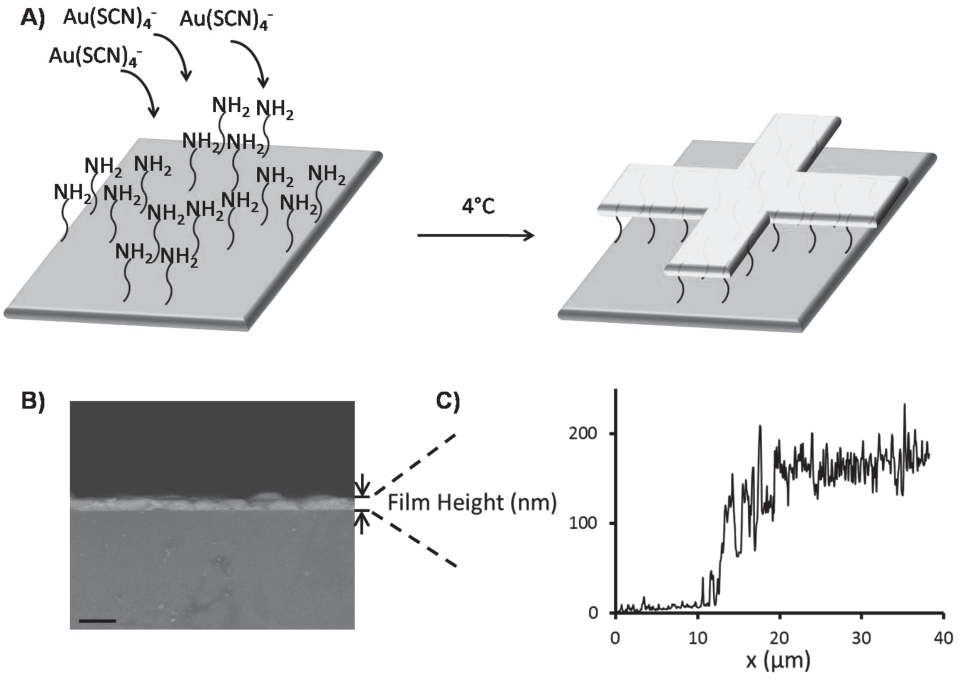

Figure 1. Formation of thin Au films. A) The experimental scheme showing an amine-patterned surface incubated with $Au(SCN)_4^{1-}$ in an aqueous solution. The thin film formed traces the contours of the amine pattern. B) Cross-section of the deposited film visualized by SEM; the film appears lighter on the silicon substrate. Scale bar corresponds to 500 nm C) AFM height profile showing an average thickness of approximately 160 nm of the deposited film (a representative film domain corresponding to the height profile is shown in Figure 1, Supporting Information).

concurrent reduction of gold into a thin nanostructured film tracing the amine patterns on the surface. Critically, no external reducing agents were needed to initiate or promote formation of the metallic Au films. Thiocyanate ligands have been previously studied as leaching agents and stabilizers of Au ions in aqueous solutions.[15,16] $Au(SCN)_4^{1-}$ complexes have been also employed as a source for gold nucleation seeds in electroless deposition pathways.[17] Here we show that $Au(SCN)_4^{1-}$ exhibits multiple roles. In essence, the thiocyanate ligands provide the means for surface targeting of the complex, guiding the Au crystallization process and, importantly, donating the reducing electrons. The Au films formed exhibit excellent electrical conductivity and high transparency in a wide spectral range.

2. Results and Discussion

The deposition procedure and morphological properties of the patterned Au films are depicted in **Figures 1** and **2.** Figure 1 illustrates the experimental scheme. $Au(SCN)_4^{1-}$ complex was synthesized through reacting $HAuCl_3$ and KSCN in water,[18] followed by incubation at 4 °C with an amine-functionalized surfaces. The process resulted in formation of surface-attached thin films (Figure 1A). The scanning electron microscopy (SEM) cross sectional image (Figure 1B) and atomic force microscopy (AFM) profile (Figure 1C) indicate that the deposited film attained a relatively uniform thickness of 160 nm ± 20 nm.

SEM data in Figure 2 present a film pattern produced following incubation of the gold complex with an amine-functionalized surface, and reveal intriguing morphological properties of the film. The SEM image in Figure 2A shows the stainless steel mask employed for producing an amine-displayed cross-shape configuration on a silicon substrate (see Experimental Section). Figure 2B displays the amine-patterned surface after incubation with $Au(SCN)_4^{1-}$. The SEM image in Figure 2B nicely demonstrates that the assembled film traced the contours of the amine coating. Closer inspection of the assembled

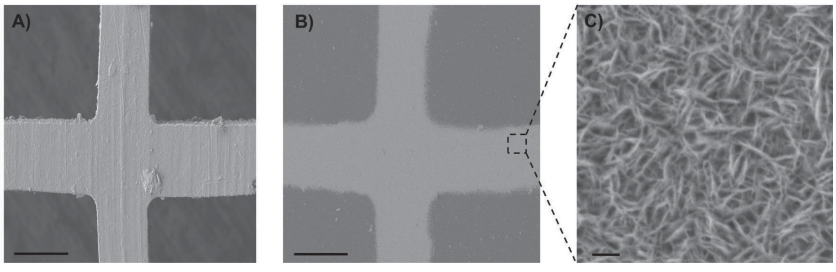

Figure 2. Patterned nanostructured film on an amine-functionalized surface. SEM images depicting the Au film pattern and film morphology. A) Metal mask designed to create the cross shape area coated with silane-amine on the silicon substrate. B) The amine-displaying surface (created with the aid of the cross-shaped mask) after incubation with $Au(SCN)_4^{1-}$; the film traced the amine-displaying domain. Scale bars in (A,B) correspond to 100 μm. C) Magnified region within the film showing the nanoribbon morphology. Scale bar 200 nm.

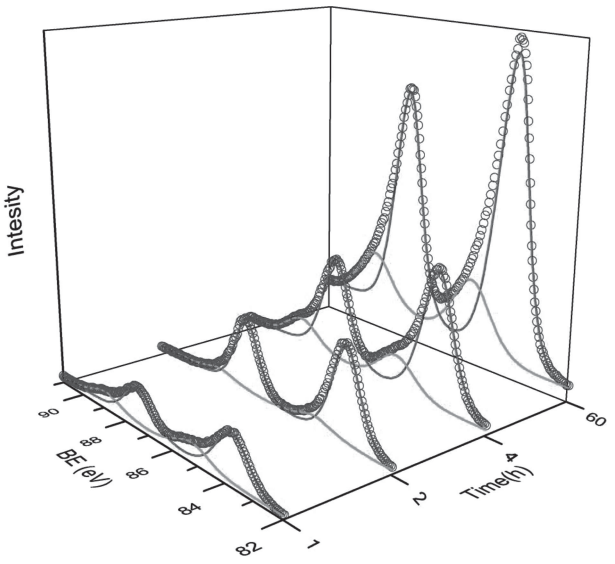

Figure 3. Au 4f species within the nanostructured film. XPS spectra depicting the relative abundance of Au species in the film. Deconvolution of the spectra shows the darker peaks (higher intensities) corresponding to Au^0 and lighter peaks (lower intensities) ascribed to Au^I.

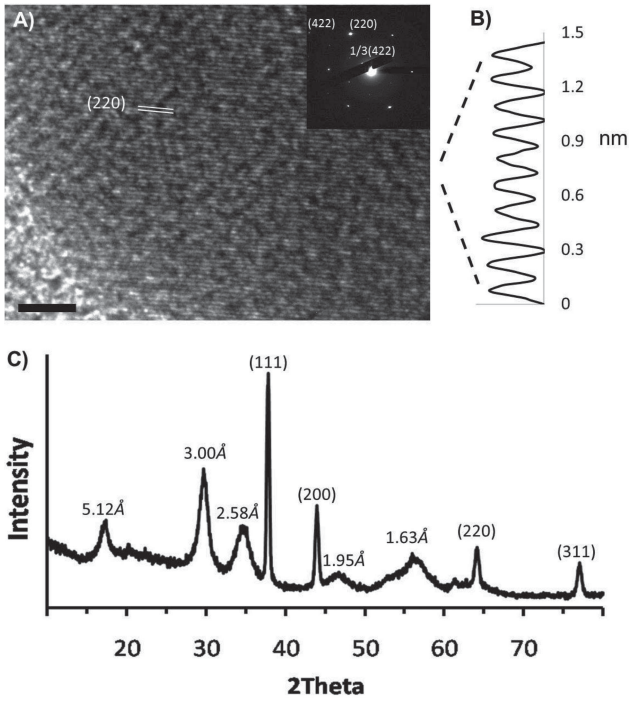

Figure 4. Crystallinity of the Au film. A) HRTEM image showing the growth of the Au ribbon in the (220) plane. Scale bar corresponds to 2 nm. Inset shows the diffraction pattern highlighting the (220) and (422) spots indicating anisotropic platelet crystalline growth. B) Line-profile of a nanoribbon cross-section emphasizing film crystallinity showing the layer spacing corresponding to the Au (220) plane. C) Powder XRD pattern of the Au film grown on amine-displayed silicon oxide for 60 h. The presence of both crystalline metallic gold [plane (111), (200), (220), and (311)], and gold/organic hybrid structures, d = 1.63 Å, 1.95 Å, 2.58 Å, 3.00 Å, and 5.12 Å, is indicated.

film reveals a dense network of nanoribbons protruding from the surface (Figure 2C). Statistical image analysis indicated that the nanoribbons exhibited lengths of 300 nm ± 30 nm, thickness of 30 nm ± 4 nm. Importantly, the nanostructured film did not detach from the surface even after prolonged washing and sonication, attesting to high affinity to the amine-functionalized surface.

To elucidate the structural features and assembly mechanisms of the films we carried out spectroscopy and microscopy experiments. X-ray photoelectron spectroscopy (XPS) experiments confirm that the nanoribbon structures comprise of predominantly metallic gold, and additional Au^I (**Figure 3**). Specifically, the XPS spectra feature superimposed peaks of Au^0 at 84.15 eV and 87.8 eV, and Au^I (85.5 eV and 89.0 eV)[19] in a ratio of approximately 4:1 [Au^0:Au^I]. Importantly, while the overall intensity of the XPS peaks gradually increased reflecting the progressive film-formation, the ratio between Au^0 and Au^I peaks remained almost constant at different incubation times. The observation of abundant Au^0 and some Au^I already after 1-hour incubation of the $Au(SCN)_4^{1-}$ with the NH_2-displaying surface is significant, indicating that reduction of Au^{III} occurred rapidly and concurrent with the binding to the amine moieties.

To investigate the crystalline properties of the gold nanostructures we examined the films with high-resolution transmission electron microscopy (HRTEM, **Figure 4**A), and X-ray diffraction (XRD, Figure 4B). The HRTEM image of a small area within an individual nanoribbon clearly demonstrates the crystalline structure of the Au film. The diffraction pattern shown in the inset in Figure 4A underscores the Au fcc crystallinity and the anisotropic structure of the nanoribbons, consistent with the appearance of the forbidden 1/3(422) spots indicating plane twinning.[20]

The sheet-like crystal growth giving rise to the Au nanoribbon morphology likely originates from aurophilic interactions between the Au^I in $Au(SCN)_2^{1-}$ complexes, formed following partial reduction of $Au(SCN)_4^{1-}$.[17] The presence of the Au^I thiocyanate complex is indeed supported by the XPS results in Figure 3. Aurophilic interactions between closed-shell Au^I atoms have been discerned in varied supramolecular systems comprising gold-complexes, giving rise to diverse morphologies, including nanowires,[19,21] and sheet-like structures.[22,23] In the system presented here, the presence of two rather small ligands (thiocyanates) in a linear configuration[24] likely facilitates planar crystalline growth giving rise to the nanoribbon assembly.

Powder XRD data presented in Figure 4C further underscore the crystalline nature of the nanoribbons and provide additional evidence for the prominence of aurophilic interactions in the film assemblies. Specifically, the diffraction peaks at 38°, 45°, 65°, and 78° correspond to the Au(111), Au(200), Au(220) and Au(311) crystal planes, respectively.[25,26] The prominent peak at around 30° reflecting the 3.00 Å plane distance is ascribed to crystalline assembly comprising $Au(SCN)_2^{1-}$ complexes bonded through aurophilic interactions,[24] while the other peaks likely correspond to partly organized crystalline structures of surface-deposited $Au(SCN)_2^{1-}$.[27]

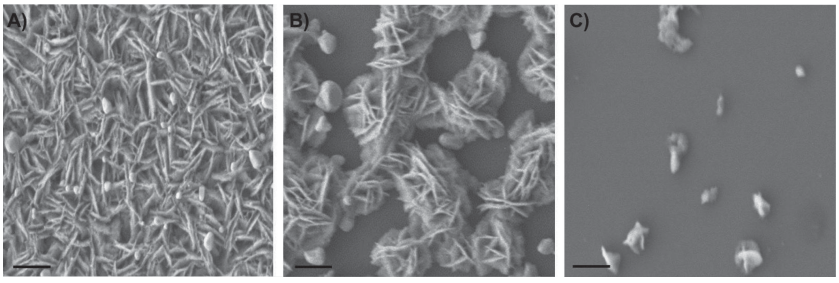

Figure 5. Effect of ionic strength upon Au film formation. SEM images show that increasing concentration of KCl inhibits film formation. A) 100 mM KCl; B) 500 mM KCl; and C) 1 M KCl. Scale bars correspond to 500 nm.

Surfaces have been previously shown to intimately participate in shaping anisotropic growth of crystalline gold, usually through surface patterns attracting Au colloids.[9,11] In the system presented here, binding of the Au thiocyanate complex to the amine residues provides the spatial framework for long-range crystalline organization through aurophilic interactions between the Au^I centers. Indeed, the appearance of anisotropic ribbon-like structures (Figure 2C) and the crystal parameters recorded in the XRD analysis (Figure 4C) both corroborate the prominent role of aurophilic interactions in the crystalline assembly.

While aurophilic interactions appear to shape film crystallinity and organization, one needs to determine the impetus for the amine-induced film formation. **Figure 5** depicts SEM images recorded following incubation of NH_2-displaying silicon substrates with $Au(SCN)_4^{1-}$ solutions containing different concentrations of KCl. The SEM data in Figure 5 show a dramatic inhibitory effect of KCl upon the formation of the Au nanostructured film. Blocking of Au film deposition through increased KCl concentrations can be ascribed to interference of the salt with the electrostatic attraction between the negatively charged complexes and the positive amine groups on the surface (as the incubation was carried out in a neutral aqueous solution and the pK_a of the short-chain amines is in the order of 10–11).[28] Similar salt-induced inhibition was observed when NaCl was added to the reaction solution (data not shown).

Supporting the conclusion regarding the central role of electrostatic attraction in film assembly was the observation that gold films did not form on thiol-coated films (data not shown). Thiol moieties, even though widely employed for binding metallic gold, are neutral in the experimental conditions used and thus did not anchor the $Au(SCN)_4^{1-}$ (or the partially reduced $Au(SCN)_2^{1-}$) complexes in the aqueous solution. Accordingly, this result indicates that the negatively charged gold thiocyanate complexes, rather than reduced gold colloids, constitute the participants in surface binding in the initial film formation step.

The experimental data presented in Figure 1–5 point to a self-assembly process progressing through several stages. Binding of the negatively charged Au-thiocyanate complexes is facilitated by electrostatic attraction to the surface-functionalized amine groups. $Au(SCN)_4^{1-}$ is concurrently reduced to $Au(SCN)_2^{1-}$, which undergo crystallization through aurophilic interactions between the Au^I atoms, with concomitant reduction of to Au^0 resulting in formation of crystalline Au nanoribbon morphology. The amine-presenting surface has a central role in directing the crystallization/reduction phenomena. Indeed, while some Au^0 colloidal particles did form spontaneously in aqueous solutions of gold thiocyanate (Figure 2, Supporting Information), they lacked the spatial, uniform film organization and were easily removed from the surface upon rinsing.

It should be emphasized that formation of the surface-deposited Au films took place without the presence of any external reducing agents–a common precondition in the large majority of gold metallization processes.[9,11] Indeed, an experiment in which a reducing agent (hydroquinone) was added to the incubation solution resulted in a significantly different outcome; hydroquinone essentially eliminated the nanoribbon film structure, but rather promoted rapid Au colloid formation in the solution (data not shown).

Particularly noteworthy is the observation that, in contrast to most Au colloid synthesis protocols, the ligand, thiocyanate in this case, is the reducing agent. Specifically, the reduction involves electron transfer from the SCN^-, likely according to equation **1**:

$$4H_2O + 2Au(III)(SCN)_4^- \rightarrow 2Au(0) + SO_4^{2-} + CN^- + 8H^+ + 7SCN^- \quad (1)$$

Several lines of evidence support this redox reaction pathway. Fourier transform infrared (FTIR) experiments confirmed the generation of sulfate moieties in the reaction mixture (Figure 3, Supporting Information). Furthermore, co-addition of H_2O_2 to the incubation solution significantly accelerated film formation and yielded complete Au^0 coverage (Figure 4, Supporting Information), explained by the fact that hydrogen peroxide promote oxidation and removal of the thiocyanate ions,[29] accordingly shifting the reaction in Equation 1 further to the products. It should be emphasized that further studies are underway in our laboratories to decipher the exact reduction reactions associated with the novel Au nanoribbon film assembly.

The unique nanoribbon thin film morphology is conducive to potential practical applications. **Figure 6**, for example, depicts the optical transparency and electrical conductivity of the gold film. Both physical properties are related to the configuration of the gold film–the protruding nanoribbons and resultant inter-ribbon spacing that together give rise to the high optical transparency (Figure 6A). Note, in particular, the significantly high transparency of the film well into the infrared (IR) spectral region–an attractive feature in varied sensing and optical devices. Similarly, excellent conductivity profile for the films is apparent (Figure 6B), recorded on a macroscopic scale (100 μm and 1 mm electrode spacings, respectively) and indicative of electron transport through the interfaces between the individual gold nanoribbon structures. The sheet resistance of the films was approximately 50 Ω sq^{-1} (Figure 6B), which is comparable to previously reported nanostructured electrodes.[30,31]

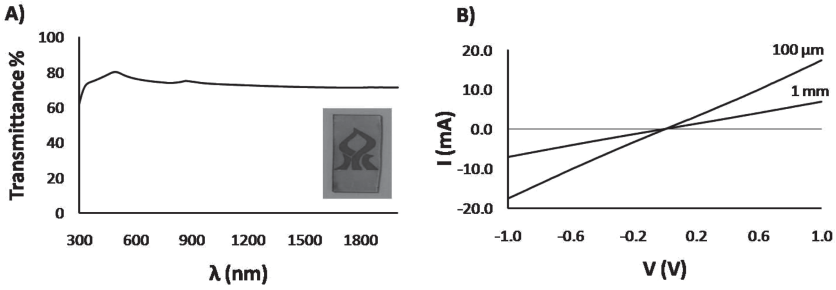

Figure 6. Physical properties of the Au films. Data recorded for Au films exhibiting similar thickness of approximately 200 nm as the film depicted in Figure 1C. A) Optical transmittance. The inset shows a picture of the Au film deposited on glass and placed upon a text feature. B) Current/voltage curve recorded for an electrode distances of 100 µm and 1 mm, respectively, underscoring high electric conductivity.

3. Conclusions

In conclusion, we have described a new technology for fabricating transparent conductive patterned films. The generic approach relies on an intriguing phenomenon in which amine-anchored $Au(SCN)_4^{1-}$ undergoes spontaneous crystallization and reduction. The function of the thiocyanate ligands in the process leading to formation of Au films is crucial. The SCN^- moieties both serve as the reducing agents, and also closely affect the crystallization properties of the film. This dual role lies at the crux of the phenomenon presented here, in which a nanostructured film, rather than assembly of Au NPs or colloids, is the predominant process taking place in solution. Indeed, different than most currently employed schemes for gold plating and gold patterning (particularly the numerous NP-based and "electroless" plating techniques), this technology is a one-step process, in which self-assembly is concomitant with reduction, overall yielding an intricate network of crystalline gold "nanoribbons" attached to the surface. Importantly, the film assembly does not require the presence of any externally added reducing agents, nor pre-deposition of metallic structures designed to serve as nucleating/catalytic sites.

Overall, the film assembly features make this new approach highly generic, and point to varied practical applications in sensing, optoelectronics, catalysis, and others. We anticipate that the Au thiocyanate-based crystallization/reduction process will be manifested for other surface-displayed functional groups other than amines, further expanding its scientific and practical scope.

4. Experimental Section

Materials and Film Deposition: $HAuCl_4$, KSCN, heptane, 3-aminopropyltriethoxysilane and hydroquinone were purchased from Sigma-Aldrich (St. Louis, MO) and used as received. DMSO (HPLC-grade) was obtained from Bio Lab Ltd (Jerusalem, Israel). 30 wt% hydrogen peroxide solution and cyclohexane were obtained from J. T. Baker (Deventer, Netherlands). The water used in the experiments were doubly purified by a Barnstead D7382 water purification system (Barnstead Thermolyne, Dubuque, IA), at 18.3 mΩ resistivity.

The $Au(SCN)_4^-$ complex was prepared according to the following procedure: 1 mL of $HAuCl_4{\cdot}3H_2O$ dissolved in water (24 mg mL^{-1}) was added to 1 mL aqueous solution of KSCN (60 mg mL^{-1}). The precipitate formed was separated by centrifugation at 4000 g for 10 min in order to separate the complex from the solution which contains KCl and excess of KSCN.

Glass or silicon wafers with amine terminal groups were prepared by immersing the substrates in a piranha solution (70% concentrated sulfuric acid and 30% hydrogen peroxide) for 30 min at 70 °C, and another 30 min under bath sonication. The substrates were then rinsed with doubly distilled water and dried using compressed air stream. The dried substrates were immersed in a 1% (volume) of 3-aminopropyltriethoxysilane in heptane solution for 1 h, after which the substrates were rinsed in cyclohexane and were left to dry prior to use. Silicon substrates were put in an ozone oven for 30 min prior to the immersion in the amino silane solution. Patterned surfaces were prepared by placing a stainless steel mask, which have a plus sign with a thickness of 100 µm, on the substrate. Then the substrate with the mask was inserted to a plasma cleaner, PDC–32G, Harrick Plasma, and the vacuum pump was turned on and work for 90 s. After 90 s the sample was exposed to plasma, at high RF, for 1 min, effectively removing all silane-amine coating outside of the mask area.

Thin films were assembled by dissolving 28 mg of $KAu(SCN)_4$ in 40 mL of water by bath-sonication for 30 min. The amine-functionalized glass/silicon substrates were inserted perpendicularly into the solution in order to reduce non-specific aggregation and incubated for up to 60 h at 4 °C. After removal, the film samples were rinsed in water and left to dry at room temperature.

SEM: For the SEM analysis films were grown on Silicon wafer (100) with a thermal oxide layer of 100 nm, modified with 3-aminopropyltriethoxysilane self-assembled monolayer. SEM images were recorded on a JEOL JSM-7400F Scanning Electron Microscope (JEOL LTD, Tokyo, Japan) at an acceleration voltage of 3 kV.

AFM: Cross section measurements were conducted by generating two perpendicular scratches on Au film grown on glass substrate using tweezers. An AFM height measurement near the edge of the scratch was then carried out. [The perpendicular scratch was aimed to ascertain that the basis from which height measurement was carried out is indeed the glass substrate]. AFM images were recorded at ambient conditions in tapping mode using a Digital Instrument Dimension 3100 mounted on an active anti-vibration table.

HRTEM: Samples were prepared using dodecylamine films compressed to surface pressure of 25 mN m^{-1} on a Langmuir trough at 20 °C, which were transferred horizontally onto 400-mesh copper formvar/carbon grids (Electron Microscope Sciences, Hatfield, PA, USA). The grids were allowed to float on aqueous solution containing $Au(SCN)_4^-$ for 1 h, after which the sample was air-dried and plasma-cleaned. HRTEM images were recorded on a 200 kV JEOL JEM-2100F. SEM analysis of the grid after 24 h confirmed that the nanostructured Au film was formed on the grid surface.

XPS: XPS analysis was carried out using Thermo Fisher ESCALAB 250 instrument with a basic pressure of 2×10^{-9} mbar. The samples were irradiated in two different areas using monochromatic Al Kα, 1486.6 eV X-rays, using a beam size of 500 µm. The high energy resolution measurements were performed with pass energy of 20 eV The core level binding energies of the Au 4f peaks were normalized by setting the binding energy for the C1s at 284.8 eV.

Powder XRD: XRD patterns were obtained using Panalytical Empyrean powder diffractometer equipped with a parabolic mirror on incident beam providing quasi-monochromatic Cu Kα radiation (λ = 1.54059 Å) and X'Celerator linear detector. Data were collected in the grazing geometry with constant incident beam angle equal to 1° in a 2θ range of 10–80° with a step equal to 0.05°.

UV-Vis and IR Spectroscopy: UV-vis and IR transmittance measurements in the range of 300 nm to 2000 nm were carried out in Caria 5000, Varian Analytical Instruments, Melbourne.

Conductivity Measurements: 100 μm square electrodes with spacings of 100 μm and 1 mm, respectively, composed of 10 nm Cr and 90 nm Au, were thermally evaporated on glass substrate onto which the Au film was deposited. Prior to the thermal evaporation the samples were inserted to a plasma cleaner, PDC - 32G, Harrick plasma, and were exposed to plasma for 2 min under vacuum. Room temperature conductivity measurements were carried out in a two-probe configuration using a probe station equipped with a Keithley 4200SCS semiconductor parameter analyzer.

Supporting Information

Supporting Information is available from the Wiley Online Library or from the author.

Acknowledgements

The authors would like to thank Prof. Ira Weinstock for helpful discussions, Dr. Taleb Mokari for transmittance measurements, and Jurgen Jopp and Roxana Golan for help with the AFM experiments.

Received: March 11, 2013
Published online: June 5, 2013

[1] A. Kumar, C. Zhou, *ACS Nano* **2010**, *4*, 11.
[2] P. Calandra, G. Calogero, A. Sinopoli, P. G. Gucciardi, *Int. J. Photoenergy* **2010**, *2010*, 1.
[3] G. M. Wallraff, W. D. Hinsberg, *Chem. Rev.* **1999**, *99*, 1801.
[4] W. Lu, C. M. Lieber, *Nat. Mater.* **2007**, *6*, 841.
[5] R. Volinsky, R. Jelinek, *Angew. Chem. Int. Ed.* **2009**, *48*, 4540.
[6] A. R. Tao, J. Huang, P. Yang, *Acc. Chem. Res.* **2008**, *41*, 1662.
[7] C. Yu, H. Nakshatri, J. Irudayaraj, *Nano Lett.* **2007**, *7*, 2300.
[8] S. Liu, R. Maoz, J. Sagiv, *Nano Lett.* **2004**, *4*, 845.
[9] B. S. Flavel, J. Yu, A. V Ellis, J. S. Quinton, J. G. Shapter, *Nanotechnology* **2008**, *19*, 445301.
[10] E. Dujardin, C. Peet, G. Stubbs, J. N. Culver, S. Mann, *Nano Lett.* **2003**, *3*, 413.
[11] A. Morag, L. Philosof-Mazor, R. Volinsky, E. Mentovich, S. Richter, R. Jelinek, *Adv. Mater.* **2011**, *23*, 4327.
[12] Z. Nie, A. Petukhova, E. Kumacheva, *Nat. Nanotechnol.* **2010**, *5*, 15.
[13] T. Thai, Y. Zheng, S. H. Ng, S. Mudie, M. Altissimo, U. Bach, *Angew. Chem. Int. Ed.* **2012**, *51*, 8732.
[14] C. R. Hansen, F. Westerlund, K. Moth-Poulsen, R. Ravindranath, S. Valiyaveettil, T. Bjørnholm, *Langmuir* **2008**, *24*, 3905.
[15] A. G. Kholmogorov, O. N. Kononova, G. L. Pashkov, Y. S. Kononov, *Hydrometallurgy* **2002**, *64*, 43.
[16] J. Li, M. S. Safarzadeh, M. S. Moats, J. D. Miller, K. M. LeVier, M. Dietrich, R. Y. Wan, *Hydrometallurgy* **2012**, *1*, 113.
[17] E. Braun, Y. Eichen, U. Sivan, *WO Patent WO/2000/025, 136*, **2006**.
[18] K. Keren, R. S. Berman, E. Buchstab, U. Sivan, E. Braun, *Science* **2003**, *302*, 1380.
[19] Z. Huo, C. Tsung, W. Huang, X. Zhang, P. Yang, *Nano Lett.* **2008**, *8*, 2041.
[20] C. Lofton, W. Sigmund, *Adv. Funct. Mater.* **2005**, *15*, 1197.
[21] X. Lu, M. Yavuz, H. Tuan, B. A. Korgel, Y. Xia, *J. Am. Chem. Soc.* **2008**, *130*, 8900.
[22] H. Schmidbaur, A. Schier, *Chem. Soc. Rev.* **2008**, *37*, 1931.
[23] H. Ecken, M. Olmstead, B. Noll, *J. Chem. Soc. Dalton* **1998**, *22*, 3715.
[24] N. L. Coker, J. K. Bauer, R. C. Elder, *J. Am. Chem. Soc.* **2004**, *126*, 12.
[25] M. Nakamoto, M. Yamamoto, M. Fukusumi, *Chem. Commun.* **2002**, *29*, 1622.
[26] M. Aslam, L. Fu, M. Su, *J. Mater. Chem.* **2004**, *14*, 1795.
[27] J. Akola, M. Walter, R. L. Whetten, H. Häkkinen, H. Grönbeck, *J. Am. Chem. Soc.* **2008**, *130*, 3756.
[28] M. B. Smith, J. March, *March's Advanced Organic Chemistry*, Wiley-VCH, Weinheim **2001**, p. 330.
[29] I. Wilson, G. Harris, *J. Am. Chem. Soc.* **1960**, *531*, 1958.
[30] D. Azulai, T. Belenkova, H. Gilon, Z. Barkay, G. Markovich, *Nano Lett.* **2009**, *9*, 4246.
[31] P. E. Lyons, S. De, J. Elias, M. Schamel, L. Philippe, A. T. Bellew, J. J. Boland, J. N. Coleman, *J. Phys. Chem. Lett.* **2011**, *2*, 3058.